Dependence of the dielectric function and electronic properties on the Co layer thickness in giant-magnetoresistance Co/Au multilayers

C. Christides
Department of Engineering Sciences, School of Engineering, University of Patras, 26110 Patras, Greece

S. Stavroyiannis and D. Niarchos
Institute of Materials Science, NCSR ''Demokritos,'' 153 10 Aghia Paraskevi, Attiki, Greece

M. Gioti and S. Logothetidis
Solid State Physics Section, Department of Physics, Aristotle University of Thessaloniki, 540 06 Thessaloniki, Greece
(Received 5 April 1999)

A series of Co/Au multilayers, which exhibit (111) texture and low-field giant magnetoresistance (GMR), were examined with spectroscopic ellipsometry (SE) in a range of Co layer thicknesses (t_{Co}). The obtained optical dielectric functions show a systematic variation with increasing t_{Co}. Analysis of the optical transitions reveals nonmonotonic variations in plasma frequency ω_p and the interband parameters with increasing t_{Co}. These anomalies in the electronic states reflect drastic changes in Co layering above 1.5 nm of t_{Co}. The complementary study of SE and GMR measurements, on similar Co/Cu and Co/Au multilayers with (111) texture, provide experimental evidence that an interplay between spin-dependent interface and bulk scattering contributions can explain the observed linear decrease of GMR with increasing t_{Co}. [S0163-1829(99)06341-9]

I. INTRODUCTION

Since the discovery of the giant-magnetoresistance (GMR) effect[1] in magnetic multilayers (MLs), both experimental and theoretical investigations are still trying to unfold the physics that governs such magnetic structures and phenomena.[2–4] The oscillatory magnetic coupling observed in GMR MLs (Ref. 5) is the key point to study this mechanism. The oscillatory magnetic coupling between ferromagnets (FMs) through a noble-metal (NM) spacer layer results from the periodicity in the appearance of spin-polarized quantum-well states at the Fermi level with varying spacer thickness.[2,3] This turns out to be equivalent to Ruderman-Kittel-Kasuya-Yosida (RKKY) theory, where the oscillation period is determined by the band structure of the NM spacer while its phase is given by bands of the ferromagnet.[2] Recently, Zahn *et al.*[6] have calculated the GMR of Co/Cu(001) multilayers and concluded that, first, quantum-well and interface states give large contributions mainly to conductivity in the plane, and second, the GMR amplitude is strongly enhanced by defects at the Co interface layer but is slightly enhanced by bulk defects in Co. Thus, spin-dependent scattering at the interfaces due to spin-polarized quantum-well states in the NM(100) (Ref. 4) has been confirmed to be responsible for the GMR effect.

However, the maximum GMR amplitude ($\approx 60\%$) at ambient conditions was observed in sputtered (polycrystalline) Co/Cu MLs (Ref. 7) with (111) texture, rather than in Co/Cu(111) superlattices[8] grown by molecular beam epitaxy (MBE), which exhibit atomically smooth interfaces favoring the creation of discrete thin-film resonance states.[2] Recent photoemission experiments revealed[4] the spatial variation of the quantum-well wave function within a Cu(100) film and confirmed that the amplitude of these spin-polarized electron waves is modulated by an *envelope* function of longer wavelength. So far, a generalized[9] RKKY model uses such an *envelope* function with wave vector $(k_{edge}-k_F)$ to reproduce the oscillatory GMR period observed in (100)-, (110)-, and (111)-textured NM spacers. However, fcc NMs with (111) texture along the growth direction of the MLs present a more complicated case than NM(100). The problem with NM(111) is that for wave vectors k_{edge}, of s,p-band edges close to the Fermi wave vectors k_F, there are no quantum-well states at the Fermi level when the parallel wave vector to [111] direction is $2k^{\parallel}=2(k_{edge}-k_F)=0$ (at the L critical point), while averaging over all finite $k^{\parallel}$ the different periods compensate each other.[2] Thus, the disagreement between the observed and calculated (with RKKY theory) oscillatory period in fcc modulated Co/Cu MLs with (111) texture[9] is due to the limited understanding of the properties of the spin-dependent electron confinement in these structures.

Another category of FM/NM(111) layered structures where RKKY theory was applied is[10] Co(0001)/Au(111) epitaxially grown MLs that exhibit perpendicular magnetic anisotropy. For this system oscillatory magnetic coupling has been reported[11] in Co/Au(111)/Co trilayers with identical Co layer thicknesses (t_{Co}) and hcp stacking, where three GMR maxima, corresponding to antiferromagnetic coupling between adjacent Co layers, were observed with increasing Au layer thickness (t_{Au}). In this system the magnetocrystalline anisotropy of hcp Co induces a large coercive field in the GMR curves[11] and the GMR amplitude ($\approx 2\%$) is an order of magnitude less than in Co/Cu(111) MLs, precluding GMR applications with epitaxial Co/Au MLs. Following the characteristic example of sputter grown Co/Cu MLs we have shown[12] that sputtered $[\mathrm{Co}(1\,\mathrm{nm})/\mathrm{Au}(2.4\,\mathrm{nm})]_{30}$ MLs with (111) texture exhibit a low-field GMR effect that make these films potential candidates for sensor applications.[13] As in sputtered Co/Cu MLs with (111) texture,[14] the intrinsic nature of antiferromagnetic coupling can be supported by

(i) the position of the GMR maximum at $t_{Au} \approx 2.4$ nm, which is similar in epitaxial hcp-Co/Au(111) layers[11] and sputtered (111) Co/Au MLs[12] with varying t_{Au}, (ii) longitudinal Kerr-effect hysteresis loops[15] in $[Co(1\,nm)/Au(2.4\,nm)]_{30}$ MLs exhibit a manifold loop that is indicative of the coexistence of bilinear and biquadratic interlayer coupling, and (iii) no detectable fraction of (100)-oriented crystallites was observed[12] in both systems.

Local structural modifications in the low-field GMR Co/Au MLs were probed with ^{59}Co nuclear magnetic resonance measurements,[16] revealing a broad distribution of magnetic hyperfine fields that cannot be assigned to any of the known crystalline or amorphous Co structures. In addition, transmission electron microscopy (TEM) measurements[17] and superlattice refinement of the x-ray spectra[12,16] have shown that (i) the layer spacing of the Au remains insensitive and close to bulk value, (ii) the Co layers are very stressed along the growth direction, with lattice spacings in the range of $0.208 \leqslant d_{111}(Co) \leqslant 0.214$ nm for $1 \leqslant t_{Co} \leqslant 3$ nm, and (iii) well-defined Co-Au interfaces, without any traces of segregation inside the columnar grains, are formed.[17]

The possible technological applications that can emerge from the large GMR ratios observed in MLs with (111) texture attract a great deal of scientific interest to investigate the elusive mechanism between the microscopic origin of the GMR phenomenon and the film morphology. In the present study our intent is to investigate both the relative changes in the joint density of electronic states nearby the Fermi surface and the changes in film morphology by varying t_{Co} in the promising GMR $[Co(t_{Co})/Au(2.4\,nm)]_{30}$ MLs. The experimental technique that was applied for the study of the optical properties is spectroscopic ellipsometry (SE), which is a nondestructive method that measures directly the complex dielectric function $\varepsilon(\omega) = \varepsilon_1(\omega) + i\varepsilon_2(\omega)$. This quantity provides information about the intraband transitions that depend on grain size effects and the interband transitions which are related to the joint density of states at high symmetry points of the Fermi surface[18,19].

II. EXPERIMENTAL DETAILS

A series of magnetron sputtered $[Co(t_{Co})/Au(2.4\,nm)]_{30}$ MLs, with nominal $t_{Co} = 0.5$, 0.7, 1, 1.2, 1.5, 2, 2.5, and 3 nm, has been deposited on Si(100) substrates covered with a 75-nm-thick SiN_x buffer layer.[12,16] The $t_{Au} = 2.5$ nm corresponds to the composition where the maximum GMR ratio ($\approx 3\%$) was reported in Co/Au MLs.[11,12] The as-deposited samples were characterized with x-ray diffraction (XRD) and cross-section TEM measurements,[12,16] where sharp interfaces and an (111)-preferred orientation is evident along the growth direction of Au. SE measurements have been carried out with a rotating analyzer spectroscopic ellipsometer, using a Xe lamp as light source. Scans were performed in the photon energy range 1.5–6.3 eV at a constant incidence angle of 67.5°, with a photon energy interval of 20 meV. SE measures the complex reflection ratio $\rho = \tan\psi\, e^{i\Delta}$. Using the measured ellipsometric angles (ψ, Δ) the $\varepsilon(\omega)$ is calculated from the complex reflectance ratio.

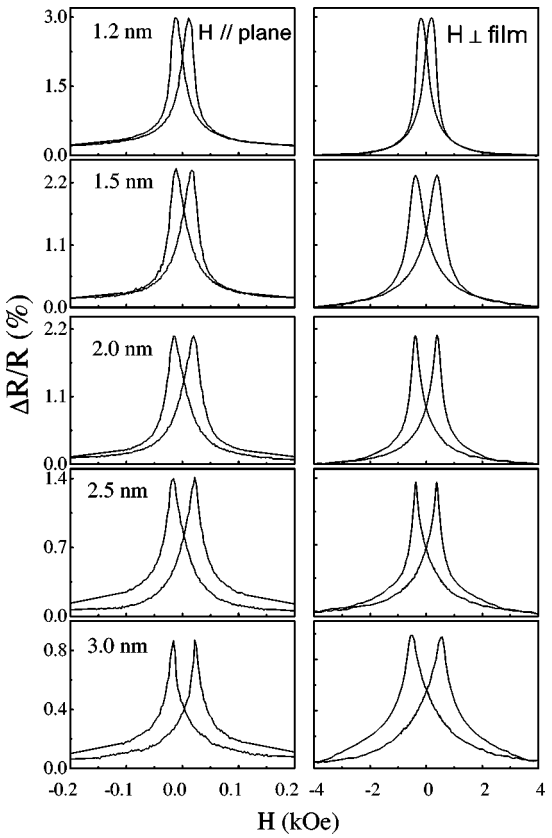

FIG. 1. On the left part are shown the GMR curves with $H \| I$ and on the right with $H \perp I$, as a function of t_{Co}.

III. GMR RESULTS

The GMR measurements were performed at 300 K with the four-point probe method, using a dc current of 1 mA for two directions of the applied field H (Fig.1): first with H lying in the film plane parallel to current ($H \| I$) and then with H applied perpendicular to film ($H \perp I$). The Co/Au MLs with $t_{Co} < 1$ nm exhibit only anisotropic magnetoresistance and are not included in Fig. 1. In Fig. 2 are shown the GMR ratios $\Delta R/R_s = (R_{max} - R_s)/R_s$, with R_{max} the maximum and R_s the minimum resistance in different magnetic fields H, as a function of t_{Co} in the $H \| I$ configuration. The obtained GMR ratios decrease quasilinearly with t_{Co}, as in GMR Co/Cu multilayers.[20] Also Fig. 2 shows that the saturation (H_s) and coercive (H_c) fields, obtained from the GMR curves with $H \| I$, approach a saturation value for thicker Co layers. The H_s values were determined from the first derivative of the GMR curves, choosing the field values where the derivative line becomes horizontal. The observed enhancement of H_c and H_s provides evidence for changes in the micromagnetic structure due to modifications in the Co layering as t_{Co} increases.

The observed GMR loops with $H \| I$ indicate that the film magnetization is lying in plane,[12] contrary to all past studies where this material combination was a typical system exhibiting a large perpendicular anisotropy[10,11] when 4–12 Co monolayers were stacked with relatively thick Au layers. Also, isothermal magnetic loops have shown[12] that the film magnetization is in plane for the examined layer thicknesses. The optimum low-field GMR is observed for $t_{Co} \approx 1$ nm and its in-plane anisotropy can be attributed[12] to Au-surface-like

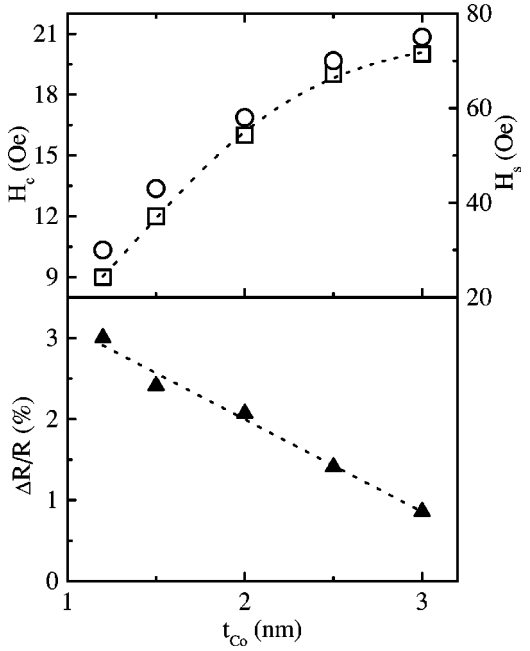

FIG. 2. The top part shows the variation of the H_c (squares) and H_s (circles) parameters from the GMR curves with $H \| I$. The corresponding GMR ratios are plotted as a function of t_{Co}. The lines are guides to the eye and the experimental error is within the size of the symbols.

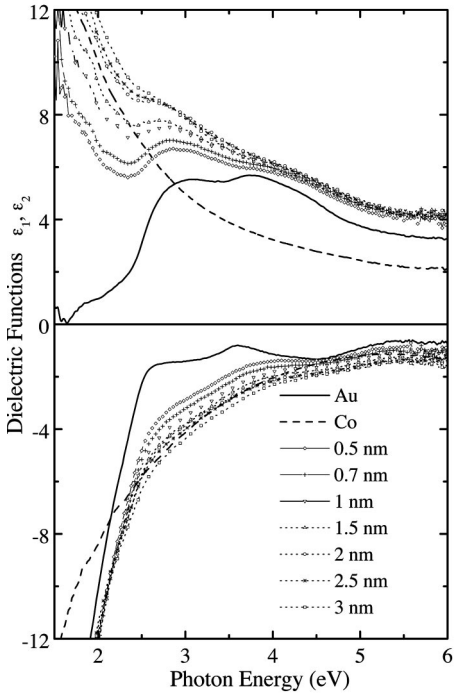

FIG. 3. The obtained real ε_1 (bottom) and imaginary ε_2 (top) parts of the dielectric function are plotted as a function of the photon energy for seven Co/Au multilayers with different t_{Co}. For clarity, the ε_1 and ε_2 values are shown in a shorter scale than the full span range between -25 and 19.

modifications induced in the Co layer structure. For $t_{\mathrm{Co}} \approx 1$ nm the coercive field H_c and the switching field H_s are 0.01 kOe and less than 0.03 kOe respectively. Comparatively, the observed[11] values in epitaxial trilayers are $H_c \approx 0.5$ kOe and H_s less than 0.05 kOe. This order of magnitude improvement of H_c and the maximum obtained GMR ratio of[12] 3%, which is about 1% higher than that observed in epitaxial trilayers,[11] indicate that such differences between the hcp Co(0001)/Au(111) trilayers[11] and our fcc Co/Au MLs (Ref. 17), arise from the different Co layer stacking[16,17] that alters the magnetocrystalline anisotropy of Co.

Conventional TEM measurements[17] reveal that our Co/Au MLs consist of columnar grains with (i) small misoriented crystals by $10°-15°$ relative to the $\langle 111 \rangle$ direction of growth and (ii) multiple twins having as twin planes the $\{111\}$ planes of growth. Their electron diffraction spectra show[17] that when the Co layers are thinner than the Au layers an average fcc lattice is formed throughout the columnar structure of the multilayer, adopting an interplanar d spacing of 0.229 nm along the growth direction. However, for $t_{\mathrm{Co}} \geqslant t_{\mathrm{Au}}$ two separate cubic lattices appear due to internal stress relaxation. Since in fcc Co the effect of magnetocrystalline anisotropy for the (111) orientation plane is much smaller than that for the (001) or (110) orientation plane,[21] the impact of crystalline anisotropy can be very different depending on the orientation of the crystallites as t_{Co} increases.

Thus far the variation of the GMR amplitude versus t_{Co} has been reconciled with phenomenological models, considering either the ratio[22] between the probability for a spin-minority electron to be scattered in the FM layer and the increasing current shunting though it or changes in the micromagnetic state[23] (misalignment of adjacent moments), which give a reduction of the GMR for thicker FM layers. The quasilinear decrease of GMR observed in Co/Au (Fig. 2) and Co/Cu MLs (Ref. 20) indicates that the GMR dependence on t_{Co} can be described by a generalized Camley-Barnas[24] model. In the quasiclassical limit[25] this model shows that the current-in-plane GMR varies linearly with $\sin^2(\theta/2)$, when θ is the angle between the magnetizations of adjacent FM layers. As we discuss in Sec. IV the linearity of GMR indicates that t_{Co} changes the degree of magnetic misalingment among the Co layers, imposing an angular dependence of GMR with t_{Co}.

IV. DIELECTRIC FUNCTION VARIATION DETERMINED FROM SE

A systematic variation of the real and imaginary parts $\varepsilon_1(\omega)$ and $\varepsilon_2(\omega)$ of the dielectric function has been observed as a function of t_{Co} (Fig. 3). In general, the $\varepsilon(\omega)$ is correlated to the electronic properties of a material. If the solid is a good conductor, like noble metals, the optical wave interacts mainly with conduction electrons, and according to the Drude model[18,19] the plasma frequency ω_p of the electron gas plays the most important role. The experimental data from the Co/Au MLs (Fig. 3) contain the low-frequency intraband or Drude contribution which is evident from the low-energy behavior before the threshold energy of the interband transitions. Because the optical constants are not available in the literature for ultrathin layers of Co and Au, it is preferable to compare the observed dielectric function of Co/Au MLs with that of pure Au or Co thin films.

The film of 100-nm-thick Au does not show the part of ε_2 that relates with intraband transitions (solid line in Fig. 3) in the low photon energy. That part of ε_2 was found[26,27] to

deviate from the Drude model, depending upon the microscopic quality of Au (purity, voids concentration, strain, grain sizes, etc.) and the film thickness. The measured absorption (ε_2) in the Au film exhibits a steep rise at about 2 eV and its yellow color is a manifestation of the rather low threshold for the excitation of $5d$-band electrons in the conduction band.[19,28] The supplementary absorption that is located below the absorption edge (≈ 1.75 eV) of Au is often observed[27] and was attributed to the presence of point defects, like vacancies, or impurities, like gas atoms, in the samples. However, a careful study[27] of Au films with different crystallographic structures has shown that neither the nature nor the location of the contributing interband transitions can be modified by important structural changes of the films. As in most earlier work[26,27] an interband onset has been resolved around 2.5 eV from the ε_1 spectrum and is followed by two peaks in ε_2 at about 3.2 and 4 eV. Empirical band calculations of the optical properties[28] reproduce qualitatively the experimental peaks. In contrast to Cu, no evidence of transitions at the X high-symmetry point is found in Au, whereas the second peak (≈ 3.2 and 4 eV) is a sum of contributions[28] from optical transitions near the L critical point for[29] Cu or Au films.

The observed dielectric function of 100-nm-thick Co film (dashed line in Fig. 3) is similar to that observed in polycrystalline Co films deposited on Si(100) substrates,[30] where the ε_1 and ε_2 exhibit a slow, almost structureless evolution. The physical origin of this phenomenon is related to the minority $3d$ bands of Co that cut by the Fermi level with complicated Fermi-surface crossings, creating numerous interband transitions.[31] Also, it was observed[32] that the formation of a surface CoO layer on Co films shifts only the reflectance curves without changing their shapes.

Generally, the observed interband peaks in SE spectra result from the varying k-space contribution. In particular, the L-high symmetry point belongs to the faces[33] where the $\langle 111 \rangle$ cubic directions intersect the fcc Brillouin zone of Au. Since the Co/Au MLs exhibit[12,16] such a preferred orientation across the growth direction, then further broadening is expected (Fig. 3) in the interband transitions of the second peak because the Fermi surface of Au intersects the Co/Au interfaces along the [111] direction. The obtained $\varepsilon_1(\omega)$ and $\varepsilon_2(\omega)$ spectra (Fig. 3) exhibit the characteristic features that generally appear[34–37] in FM/NM MLs, with NM=Cu or Pd.

(i) Both the real and imaginary parts of $\varepsilon(\omega)$ show a monotonic, systematic shift with increasing t_{Co}, moving from Au-like optical constants to Co-like constants.

(ii) The $\varepsilon_1(\omega)$ and $\varepsilon_2(\omega)$ spectra exhibit an interband peak at about 2.5 eV and a second broad feature at about 4 eV, in qualitative agreement with our polar Kerr rotation spectra[14] and spectra of epitaxially grown Co(0001)/Au(111) MLs (Ref. 34) or sandwiched[35] structures.

(iii) The large interband broadening that is observed in Au based MLs, compared to the sharp threshold absorption edge of pure Au film, arises from symmetry breaking at the interfaces of the multilayer and extra broadening of the intraband contributions due to confinement of the electronic mean free path from grain boundaries.

V. ANALYSIS OF THE SE SPECTRA

A phenomenological expression that takes into account the free-carrier and photon absorption from intraband and interband electron transitions was used to fit the observed dielectric function of the Co/Au MLs. The $\varepsilon(\omega)$ fitting function is written[20,38] as the sum of a Drude term plus a damped Lorentzian oscillator term, centered at the low-energy interband peak position ($h\omega_0/2\pi$) with a strength A and a damping (broadening) factor γ. A second Lorentzian term was used for the feature near 4 eV, to take into account the vast peak broadening in this range. The analytical expression contains a constant background term ε_∞ as well:

$$\varepsilon(\omega)=\varepsilon_\infty-\omega_p^2/(\omega^2+i\omega\Gamma)+A/(\omega_0^2-\omega^2-i\gamma\omega). \quad (1)$$

In the second (Drude) term $\omega_p=(4\pi N_c e^2/m^*)^{1/2}$ is the unscreened plasma energy related to the density N_c of the free carriers with m^* being the effective optical mass and Γ ($\approx 1/\tau_{eff}$) being the broadening parameter, which is inversely proportional to the free-carrier effective[27] scattering time τ_{eff}. A quantitative estimation of ω_p, Γ, the energy peak position, the amplitude—which depends upon the strength factor A—and the broadening γ parameters is achieved by simultaneous least-squares fitting of the real and imaginary parts of the $\varepsilon(\omega)$ spectra. The obtained plasma energy ω_p (top) and broadening Γ (bottom) parameters are plotted in Fig. 4 against t_{Co}. For comparison, the ω_p and Γ parameters obtained[20] from similar Co/Cu MLs are shown in Fig. 4. It is obvious that (i) there is a distinct difference between the Co/Cu and Co/Au MLs on the variation of ω_p with t_{Co} and (ii) the broadening parameter Γ for the Co/Au MLs is almost twice the value of the corresponding Co/Cu MLs.

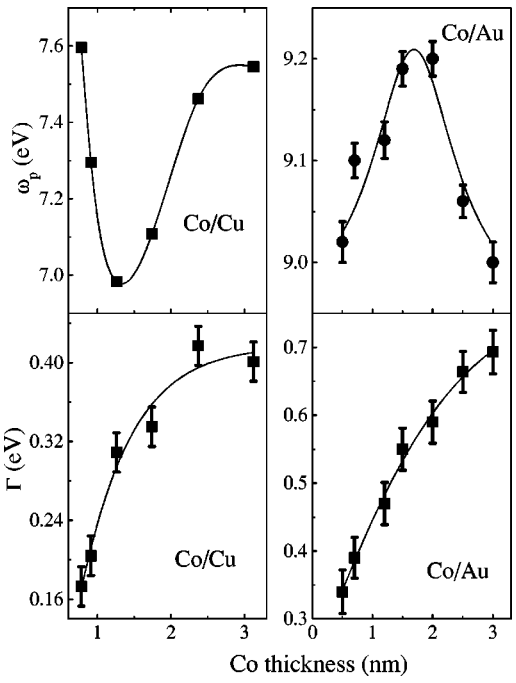

FIG. 4. The estimated values of the plasma energy ω_p and the Drude broadening parameter Γ, from Eq. (1), are plotted as a function of the nominal t_{Co} values for the (Ref. 20) Co/Cu and Co/Au MLs. The lines are guides to the eye and the experimental error is within the size of the symbols for the ω_p of Co/Cu.

To enhance the existing structure in the spectra we calculate numerically the second derivative $d^2\varepsilon/d\omega^2$ of the complex dielectric function from our ellipsometric data.[39] From this process only one interband feature in $d^2\varepsilon/d\omega^2$ was well resolved to allow a quantitative analysis with standard spectral line shapes,[18] considering a mixture of a two-dimensional (2D) minimum with a saddle critical point:[39]

$$\varepsilon(\omega)=C-A_{CP}e^{i\phi}\ln(E_{CP}-\omega-i\Gamma_{CP}). \tag{2}$$

The derivative spectra were fitted to one-electron critical point line shapes. A least-squares procedure was used, where both the real and imaginary parts of $d^2\varepsilon/d\omega^2$ were fitted simultaneously. Fits of the experimental second derivative $\varepsilon_1''(\omega)$, $\varepsilon_2''(\omega)$ spectra were performed with functions of the second derivative:

$$\varepsilon_1''(\omega)=-A_{CP}e^{i\phi}(E_{CP}-\omega-i\Gamma_{CP})^{-1},$$

$$\varepsilon_2''(\omega)=-A_{CP}e^{i\phi}(E_{CP}-\omega-i\Gamma_{CP})^{-2}, \tag{3}$$

where the angle ϕ represents the amount of mixing ($0<\phi<\pi/2$). Thus, $\phi=0$ corresponds to a minimum (M_0), $\phi=\pi/2$ to a saddle point, and $\phi=\pi$ to a maximum (M_3) critical point.[18] A_{CP} is the amplitude parameter that is proportional to the strength of the oscillator, E_{CP} is the critical point energy, Γ_{CP} its broadening parameter, and C is a constant. In Fig. 5 is shown the variation of E_{CP}, A_{CP}, Γ_{CP}, and ϕ with t_{Co}, including the corresponding parameters from the pure Au film as well ($t_{\mathrm{Co}}=0$).

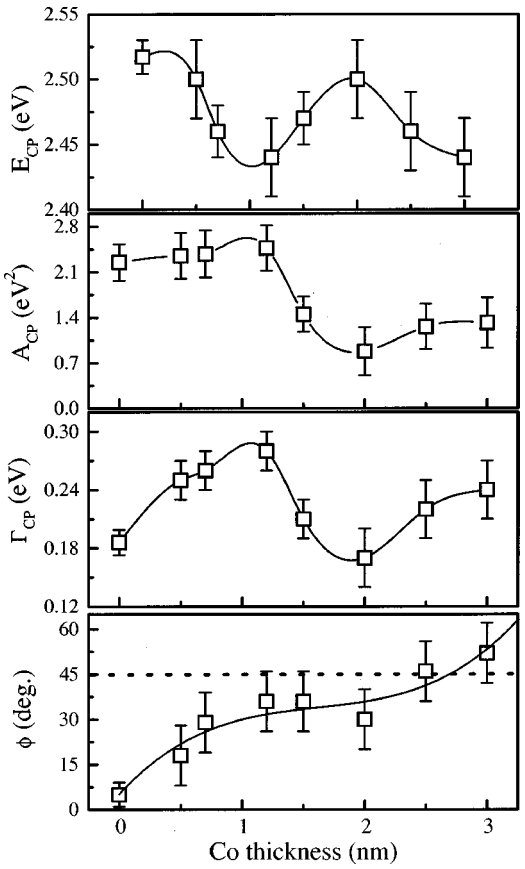

FIG. 5. The variation of the estimated parameters [Eq. (3)] E_{CP}, A_{CP}, Γ_{CP}, and ϕ with t_{Co}, including the corresponding parameters from the pure Au film as well ($t_{\mathrm{Co}}=0$), is shown. The solid lines are guides to the eye.

VI. DISCUSSION AND CONCLUSIONS

First of all, the physical origin of the observed trend in Figs. 3 and 4 is discussed below. It was shown[27] that Γ depends upon the optical relaxation time τ_0 ($\tau_{eff}\propto[\tau_o+O\omega^n]$). The τ_0 is very sensitive to the presence of volume defects (grain boundaries, imperfections, and impurities inside the grains), degree of specular reflection of the electrons on interfaces, and anomalous skin-effect corrections from surface defects. Thus, a comparison among the absolute values of Γ may lead to ambiguous conclusions. Moreover, if we consider a change of the relaxation time that takes into account a correction for the film thickness[34] and write the $\Gamma=(\xi/\lambda\tau)$, where ξ is the mean free path in the bulk and λ is the restricted mean free path in the MLs, then from Fig. 4 the ratio $(\Gamma_{\mathrm{Au}}/\Gamma_{\mathrm{Cu}})\propto(\lambda_{\mathrm{Cu}}/\lambda_{\mathrm{Au}})>1$ emerges for every t_{Co}.

Since the Co/Cu and Co/Au layer thicknesses are the same as a function of t_{Co}, the involved approximation concerns only the ratio ξ/τ, considering that there is no difference between Cu and Au layers. This is a reasonable assumption because Cu and Au exhibit Fermi surfaces with comparable ratios of ''belly'' to ''neck'' orbits, according to de Haas–van Alphen data,[40] and have the same Drude relaxation times ($\approx 2.8\times10^{-14}$ sec) at room temperature. The $(\lambda_{\mathrm{Cu}}/\lambda_{\mathrm{Au}})>1$ condition indicates that a larger *spin-independent* scattering occurs in Co/Au MLs. Thus, the larger GMR amplitude observed[20] in Co/Cu MLs (grown under the same deposition conditions) than in Co/Au MLs is in agreement with this finding.

In the examined photon energy range the major contribution to ω_p arises from the Au or Cu layers despite the fact that only the t_{Co} is varied (Fig. 4). However, only in Co/Au MLs are the ω_p values very close to $\omega_p(\mathrm{Au})\approx 9.22$ eV for pure Au films[35] whereas in Co/Cu MLs they are well below the $\omega_p(\mathrm{Cu})\approx 8.4$ eV of pure Cu for all the examined t_{Co} region. Since $\omega_p^2\propto(N_c/m^*)$, with the optical mass[19,27] lying between $0.94\leqslant m^*_{\mathrm{Au}}\leqslant 1.05$ for pure Au and $1.32\leqslant m^*_{\mathrm{Cu}}\leqslant 1.45$ for pure Cu, it is reasonable to assume that the observed variation of ω_p in Fig. 4 is related mainly to changes of N_c. Variations of N_c can be explained either with changes in the distribution of grain sizes[29] and/or structural modifications (internal stress effects) in layering for thicker MLs. This conclusion can be drawn from the reversal of the nonmonotonic variation of ω_p with t_{Co} (Fig. 4) when the Cu layers are replaced by Au. Specifically, both systems exhibit a nonmonotonic variation, where the ω_p decreases for $t_{\mathrm{Co}}<1.5$ nm and increases for $t_{\mathrm{Co}}>1.5$ nm in Co/Cu, while the opposite behavior is observed below and above the $t_{\mathrm{Co}}=2$ nm in Co/Au MLs. The nonmonotonic variation can be related to changes in the grain size distibution as a function of t_{Co}. Indeed, cross-section TEM images[17] show that the morphology of the columns in our Co/Au MLs is more spiked for $t_{\mathrm{Co}}>2$ nm. Also planar view micrographs show a bimodal distribution of grain sizes with a larger fraction of small grains relative to multilayers with $t_{\mathrm{Co}}\leqslant 2$ nm.

The obtained variation of intraband parameters in Fig. 4 coincides with the t_{Co} region where the obtained H_s and H_c fields from the GMR curves increase for the[20] Co/Cu and

Co/Au MLs (Fig. 2). These results together with the observed TEM differences between[41] Co/Cu and Co/Au MLs (Ref. 17) indicate that the reverse variation of ω_p is due to layer modifications in the two systems. Such differences between Co/Cu and Co/Au MLs with (111) texture can be initiated by the lattice mismatch at the interfaces, which is about 2% and 15%, respectively, and the unique ability of Au layers to minimize the stress at the interface during the growth[42] of Co on Au(111) with a mechanism that is known as surface reconstruction.[43]

The steep rise of $\varepsilon_2(\omega)$ in Au (Fig. 3) is due to the optical plasma resonance absorption edge that is sensitive[29] to grain-size effects as well. The observed (Fig. 3) smearing of the Au resonance edge and broadening of Au interband transitions with increasing t_{Co} is comparable with the reported size-dependent change in interband transitions[29] of Cu or Au nanoparticles. The reported changes in transmittance optical spectra were associated with an increase in the curvature of the d levels due to reduced $N(E_F)$ at the surface with decreasing size of Cu particles.[29] In our case, the analysis of the interband transitions indicates that there is a modification of the joint density of electronic states inside the NM layers of Co/Au and Co/Cu MLs as a function of t_{Co}. Since the Co layers expand significantly along the growth direction for thinner Co layers,[16,17] then a change of $N(E_F)$ can be associated with changes in Co layer density at the Co/Au interfaces as their lattice relaxes from an Au-surface-like to a Co-bulk-like structure[17] with increasing t_{Co}. TEM measurements[17] in our Co/Au MLs show clearly that for $t_{\mathrm{Co}} \leqslant 2$ nm the Co lattice is expanded by 4.4% relative to bulk value while the Au lattice is compressed along the growth direction. As a result an average fcc lattice between Co and Au layers was observed. For thicker Co layers the fcc Co lattice is expanded by 2.9% along the growth direction whereas no average lattice is formed in this case and both elements exhibit interplanar spacings close to their bulk values.

The obtained variation of ϕ together with the nonmonotonic behavior of the interband parameters (Fig. 5) indicates that the band pairs of Au exhibit a change in the singular behavior from a minimum critical point in pure Au ($\phi \approx 5°$) to a mixture of a minimum with a saddle point in the range between $1 < t_{\mathrm{Co}} < 2$ nm ($20° < \phi < 40°$) that transforms to a pure saddle critical point for $t_{\mathrm{Co}} > 2$ nm ($\phi \approx 45°$). Such changes near the high-symmetry lines of the band structure are directly related to changes in the curvature of the upper $5d$ conduction band of Au, which can be reconciled with effective-mass theory. It is worth mentioning here that the m^* in ω_p is the free-electron mass from states near the bottom of the s,p conduction band, whereas the curvature changes near interband transitions correspond to effective masses from the top of the conduction band. Previous studies of the quantum-well states in Cu films deposited[44] on fcc Co(001) and Ag films on Fe(001) have shown an enhancement of the effective masses relative to the free-electron mass as a function of the NM layer thickness. Such changes were attributed to a strong modification in the Fermi-surface crossings of the quantum-well states by a strong hybridization with the d bands of the FM layer.[44] The theory explains how[3,45] spin-dependent electron confinement helps the formation of spin-polarized quantum-well states in NM(100) spacers. The spin polarization of NM(100) levels was explained in terms of the spin-dependent reflectivities at the FM/NM interface. For the high symmetry direction $k^{\parallel} = 0$ (along the ΓX direction) of fcc Co, the spin-minority Δ_1 d band hybridizes with the s,p bands[2,3] and creates a gap in the vicinity of E_F. This gap defines the degree of confinement of the quantum-well state in NM, where propagating waves will be reflected back into the spacer layer. Since for the majority band structure the hybridization gap is displaced to higher binding energies and the majority NM spin states in the vicinity of E_F become less strongly confined, then the quantum-well states that survive in NM(100) carry minority spin.

In GMR MLs with NM(111) spacers there are no spin-polarized quantum-well states[2] for $k^{\parallel} = 0$ near the E_F at the L critical point. But, most important, there is no sd hybridization along the [111] direction as in the Δ_1 d band of fcc Co(100). Thus contrary to Cu/Co(100) layers [Ref. 4(b)], in the case of (111) texture there should not be quantum-well interference due to multiple electron reflections within the FM layer. Consequently, an increase of t_{Co} should affect in a different way the magnetotransport properties of the examined Co/Au and[20] Co/Cu MLs because the specular reflections of the electron waves on interface potential steps are reduced. The SE spectra as a function of t_{Co} provide experimental evidence for changes in $N(E_F)$ (Fig. 5) and ω_p (Fig. 4) due to changes in Co layering.[16,17] Such changes in Co layering can cause larger interface roughness, giving a significant contribution to interface resistance,[46] which implies a smaller contribution from the interface potential steps and therefore smaller step heights for thicker Co layers. A semiclassical model that solves the Boltzmann equation[25] taking into account spin-dependent electron scattering on impurities as well as on interfacial roughness predicts a linear variation of the current-in-plane GMR with $\sin^2(\theta/2)$. Within the semiclassical approach[25] the angular variation of GMR leads always to a linear dependence on $\sin^2(\theta/2)$ when either bulk or interface scattering is considered as the origin of the GMR effect. Thus the observed quasilinear decrease of GMR (Fig. 2) can be understood as a progressive increase of misalignment between the magnetic components of adjacent Co layers with increasing t_{Co}. The proposed angular dependence of GMR on t_{Co} is equivalent to contributions from biquadratic interlayer coupling, observed[41] in low-field GMR Co/Cu MLs due to a progressive increase of magnetic misalignment by changes in film morphology.

In conclusion, the use of SE has made possible to measure the concerted action of the developed film morphology and spin-dependent electronic structure at the Fermi level in fcc modulated Co/Au and Co/Cu MLs with (111) texture. In this way we brought into light common microstructural and electronic aspects that affect the depedence of the magnetotransport properties on t_{Co}. Both Co/Au and[20] Co/Cu MLs exhibit a quasilinear decrease of the GMR amplitude with increasing t_{Co}. Also, an enhancement of the H_c and H_s values coincides with the t_{Co} range where the intraband and interband parameters in Figs. 4 and 5 exhibit extrema. These results indicate that both low-field GMR Co/Cu and Co/Au MLs exhibit drastic changes in Co layering at $t_{\mathrm{Co}} \approx 1.5$ nm. Since for larger t_{Co} values very small GMR amplitudes were

observed, then the SE measurements determine the t_{Co} values where changes in the Co layer roughness increase the interface resistance considerably. As a consequence the smaller contribution from the interface potential steps reduces the spin-dependent scattering at interfaces and, within the limits of the semiclassical approximation,[24,25] drive an interchange of GMR contributions from interface to bulk scattering with increasing t_{Co}.

[1] M. N. Baibich, J. M. Broto, A. Fert, F. Nguyen Van Dau, F. Petroff, P. Etienne, G. Creuzet, A. Friederich, and J. Chazelas, Phys. Rev. Lett. **61**, 2472 (1988).

[2] J. E. Ortega, F. J. Himpsel, G. J. Mankey, and R. F. Willis, Phys. Rev. B **47**, 1540 (1993).

[3] P. Lang, L. Nordstrom, W. Wilderberger, R. Zeller, P. H. Dederichs, and T. Hoshino, Phys. Rev. B **53**, 9092 (1996).

[4] (a) R. K. Kawakami, E. Rotenberg, H. J. Choi, E. J. Escorcia-Aparicio, M. O. Bowen, J. H. Wolfe, E. Arenholz, Z. D. Zhang, N. V. Smith, and Z. Q. Qiu, Nature (London) **398**, 132 (1999); (b) R. K. Kawakami, E. Rotenberg, E. J. Escorcia-Aparicio, H. J. Choi, T. R. Cummins, J. G. Tobin, N. V. Smith, and Z. Q. Qiu, Phys. Rev. Lett. **80**, 1754 (1998).

[5] S. S. P. Parkin, R. Bhadra, and K. P. Roche, Phys. Rev. Lett. **66**, 2152 (1991).

[6] P. Zahn, J. Binder, I. Merting, R. Zeller, and P. H. Dederichs, Phys. Rev. Lett. **80**, 4309 (1998).

[7] S. S. P. Parkin, Z. G. Li, and D. J. Smith, Appl. Phys. Lett. **58**, 2710 (1991).

[8] M. J. Hall, B. J. Hickey, M. A. Howson, M. J. Walker, J. Xu, D. Creig, and N. Wiser, Phys. Rev. B **47**, 12 785 (1993).

[9] P. Bruno and C. Chappert, Phys. Rev. Lett. **67**, 1602 (1991); **67**, 2592 (1991); Phys. Rev. B **46**, 261 (1992).

[10] E. Velu, C. Dupas, D. Renard, J. D. Renard, and J. Seiden, Phys. Rev. B **37**, 668 (1988).

[11] V. Grolier, D. Renard, B. Bartelian, P. Beauvillain, C. Chappert, C. Dupas, J. Ferre, M. Galtier, E. Kolb, M. Mulloy, J. P. Renard, and P. Veilet, Phys. Rev. Lett. **71**, 3023 (1993).

[12] S. Stavroyiannis, C. Christides, D. Niarchos, Th. Kehagias, Ph. Komninou, and Th. Karakostas, J. Appl. Phys. **84**, 6221 (1998).

[13] C. Christides, S. Stavroyiannis, G. Kallias, A. G. Nassiopoulou, and D. Niarchos, Sens. Actuators A (to be published).

[14] R. Coehoorn, M. T. Johnson, W. Folkerts, S. T. Rurcell, N. W. E. McGee, A. De Veirman, and P. J. H. Bloemen, *Magnetism and Structure in Systems of Reduced Dimension*, Vol. 309 of *NATO Advanced Study Institute, Series B: Physics*, edited by R. F. C. Farrow, B. Dienny, M. Donath, A. Fert, and B. D. Hermsmeier (Plenum, New York, 1993), p. 295.

[15] C. Christides, R. Lopusnik, J. Mistrik, S. Stavroyiannis, and S. Visnovsky, J. Magn. Magn. Mater. **198-199**, 36 (1999).

[16] C. Christides, S. Stavroyiannis, D. Niarchos, M. Wojcik, S. Nadolski, and E. Jedryka, Phys. Rev. B **59**, 8812 (1999).

[17] Th. Kehagias, Ph. Komninou, C. Christides, S. Stavroyiannis, and Th. Karakostas, J. Cryst. Growth (to be published).

[18] M. Cardona, in *Modulation Spectroscopy*, Supplement 11 of *Solid State Physics*, edited by F. Seitz, D. Turnbull, and H. Ehrenreich (Academic, New York, 1969).

[19] P. O. Nilsson, in *Solid State Physics*, edited by H. Ehrenreich, F. Seitz, and D. Turnbull (Academic, New York, 1974), Vol. 29, p. 139.

[20] C. Christides, S. Logothetidis, M. Gioti, S. Stergioudis, S. Stavroyiannis, and D. Niarchos, J. Appl. Phys. **83**, 7757 (1998).

[21] Y. Zheng and J.-G. Zhu, J. Appl. Phys. **85**, 4776 (1999).

[22] C. Cowache, B. Dieny, A. Chamberod, D. Benizri, F. Berthet, S. Auffret, L. Giacomoni, and S. Nossov, Phys. Rev. B **53**, 15 027 (1996).

[23] Z. J. Yang and M. R. Scheinfein, Phys. Rev. B **52**, 4263 (1995).

[24] R. E. Camley and J. Barnas, Phys. Rev. Lett. **63**, 664 (1989); J. Barnas, A. Fuss, R. E. Camley, P. Grundberg, and W. Zinn, Phys. Rev. B **42**, 8110 (1990).

[25] J. Barnas, O. Baksalary, and A. Fert, Phys. Rev. B **56**, 6079 (1997).

[26] D. E. Aspnes, E. Kinsborn, and D. D. Bacon, Phys. Rev. B **21**, 3290 (1980).

[27] M. I. Theye, Phys. Rev. B **2**, 3060 (1970).

[28] R. Lasser, N. V. Smith, and R. L. Benbow, Phys. Rev. B **24**, 1895 (1981).

[29] E. Anno, M. Tanimoto, and T. Yamaguchi, Phys. Rev. B **38**, 3521 (1988).

[30] C. Viguier, A. Cros, A. Humbert, C. Ferrieu, O. Thomas, R. Madar, and J. P. Senateur, Solid State Commun. **60**, 923 (1986).

[31] J. H. Weaver, E. Colavita, D. W. Lynch, and R. Rosei, Phys. Rev. B **19**, 3850 (1979).

[32] Y-C. Yu, T. M. Donovan, and W. E. Spicer, Phys. Rev. **167**, 670 (1968).

[33] P. Heimann, H. Miosga, and H. Neddermeyer, Phys. Rev. Lett. **42**, 801 (1979).

[34] R. Atkinson, W. R. Hendren, I. W. Salter, and M. J. Walker, J. Magn. Magn. Mater. **130**, 442 (1994).

[35] S. Visnovsky, M. Nyvlt, V. Prosser, J. Ferre, G. Penissard, D. Renard, and G. Sczigel, J. Magn. Magn. Mater. **128**, 179 (1993).

[36] S. Uba, L. Uba, A. Ya Perlov, A. N. Yaresko, V. N. Antonov, and R. Gontarz, J. Phys.: Condens. Matter **9**, 447 (1997).

[37] S. Logothetidis, J. Petalas, N. K. Flevaris, and R. L. Johnson, Thin Solid Films **234**, 538 (1993).

[38] S. Logothetidis and N. K. Flevaris, J. Appl. Phys. **75**, 7978 (1994).

[39] L. Vina, S. Logothetidis, and M. Cardona, Phys. Rev. B **30**, 1979 (1984).

[40] P. T. Coleridge and I. M. Templeton, Phys. Rev. B **25**, 7818 (1982).

[41] C. Christides, S. Stavroyiannis, N. Boukos, A. Travlos, and D. Niarchos, J. Appl. Phys. **83**, 3724 (1998).

[42] B. Voigtlander, G. Meyer, and N. M. Amer, Phys. Rev. B **44**, 10 354 (1991).

[43] J. V. Barth, H. Brune, G. Ertl, and R. J. Behm, Phys. Rev. B **42**, 9307 (1990).

[44] P. D. Johnson, K. Garrison, Q. Dong, N. V. Smith, D. Li, J. E. Mattson, J. Pearson, and S. D. Bader, Phys. Rev. B **50**, 8954 (1994); C. Carbone, E. Vescovo, R. Klasges, W. Eberhardt, O. Rader, and W. Gubat, J. Appl. Phys. **76**, 6966 (1994); N. B. Brookes, Y. Chang, and P. D. Johnson, Phys. Rev. B **50**, 15 330 (1994); P. D. Johnson, Rep. Prog. Phys. **60**, 1217 (1997).

[45] J. Mathon, A. Umerski, M. Villeret, and R. B. Muniz, Phys. Rev. B **59**, 6344 (1999).

[46] J. Barnas and A. Fert, Phys. Rev. B **49**, 12 835 (1994).